アカデミックプログラム［B講演］ | 19. コロイド・界面化学：口頭B講演

2025年3月27日(木) 9:30 ~ 11:40 [C]C507(第2学舎 2号館 [5階] C507)

[[C]C507-2am] 19. コロイド・界面化学

座長：秋山 毅、西 弘泰

日本語
9:30 ~ 9:50
[[C]C507-2am-01]
トポタクティック反応による*hcp*-Pdナノ粒子の合成

○松本 憲志[1]、寺西 利治[1,2] (1. 京都大学化学研究所、2. 京都大学大学院理学研究科)

英語
9:50 ~ 10:10
[[C]C507-2am-02]
$B8_1$型異方性結晶構造をもつナノ粒子の合成と可視局在表面プラズモン共鳴特性評価

○LEE HYUNJI[1]、竹熊 晴香[1,2]、佐藤 良太[2]、飯田 健二[3]、寺西 利治[1,2] (1. 京大院理、2. 京大化研、3. 北大触媒化学研)

英語
10:10 ~ 10:30
[[C]C507-2am-03]
クエン酸イオンで保護された銀ナノ粒子の遠心分級とSERS基板への応用

○小山 奈津季[1]、奥 健夫[2]、秋山 毅[2] (1. 滋賀県大院工、2. 滋賀県大)

10:30 ~ 10:40
休憩

日本語
10:40 ~ 11:00
[[C]C507-2am-04]
コロイドナノ粒子からの溶媒依存的な表面リガンド除去：被覆率と分散性の変化

○山下 翔平[1]、佐川 真彦[1]、岡田 洋平[1] (1. 東京農工大学)

英語
11:00 ~ 11:20
[[C]C507-2am-05]
Highly Photoluminescent $PdAu_{12}$ and $PtAu_{12}$ Clusters Protected by Bidentate N-Heterocyclic Carbenes

○Dennis Alexander Buschmann[1,2], Shinjiro Takano[1,2], Tatsuya Tsukuda[1,2] (1. The University of Tokyo, 2. Queen's University)

英語
11:20 ~ 11:40
[[C]C507-2am-06]
Phase Separation of Epsilon Iron Oxide and Barium Ferrite using a Reverse-Micelle and Sol-Gel Combined Synthesis

○Jessica Grace MacDougall[1], Hiroko Tokoro[2], Marie Yoshikiyo[1], Asuka Namai[1], Shin-ichi Ohkoshi[1] (1. The University of Tokyo, Graduate School of Science, 2. The University of Tsukuba, Faculty of Pure and Applied Sciences)

トポタクティック反応による *hcp*-Pd ナノ粒子の合成

（京大化研[1]・京大院理[2]）○松本 憲志[1]・寺西 利治[1,2]
Synthesis of *hcp*-Pd nanoparticles via topotactic reaction ([1]*Institute for Chemical Research, Kyoto University,* [2]*Graduate School of Science, Kyoto University*) ○Kenshi Matsumoto[1], Toshiharu Teranishi[1,2]

Crystal structure of a monometal is a crucial factor for determining its physicochemical properties, and the development of metastable phases is an important means to control the properties. However, synthesizing the metastable phases has been still challenging. Here, we considered that an increase of valence electrons in a Pd-based compound could form an *hcp*-Pd sublattice according to Hume-Rothery's electron concentration law to give a metastable *hcp*-Pd phase via topotactic reaction. To facilitate the topotactic reaction, we used carbon atoms as a stabilizer of the *hcp*-Pd sublattice despite that the thermodynamically stable phase of PdC_x (x < 0.15) is only *fcc*-Pd sublattice. For this purpose, we need to kinetically synthesize the Pd–C compound containing more amount of carbon. We will present the formation of *hcp*-Pd sublattice and *hcp*-Pd metastable phases by introducing and withdrawing carbon, respectively.
Keywords : hcp-Pd; Topotactic reaction; Carbon; Metastable phase; Kinetic formation

金属の結晶構造はその物理的・化学的な特性を決定する主要因子であり、準安定相の開拓はその物質の特性を制御する上で重要な手段である。しかし、準安定相の戦略的合成は依然として挑戦的課題である。Hume-Rothery 電子濃度則[1]に従えば、Pd 基化合物の価電子数の増加により *hcp*-Pd 副格子が安定化される可能性があることから、トポタクティック反応による準安定相 *hcp*-Pd の合成を着想した。本研究では、C 原子の導入・引き抜きによる戦略的な準安定相 *hcp*-Pd ナノ粒子の合成を行った（図 1）。

PdC_x（x < 0.15）の熱力学的安定相は Pd 副格子が *fcc* 相のみのため[2]、更なる価電子数の増加のために C 導入量の多い Pd–C 化合物を速度論的に形成する必要がある。そこで、C 原子の Pd 格子内への拡散を容易にするために、非晶質 Pd–S ナノ粒子への C 導入を行った。その結果、粉末 XRD 測定により *hcp*-Pd 副格子の形成が確認され、EDX 元素マッピングにより S の粒子外への溶出が観察された。次に、空気下での *in situ* XRD 測定により *hcp* 型 Pd 副格子の構造変化を確認したところ、250 °C 付近まで格子が収縮する挙動が確認された。この結果は、*hcp*-Pd 格子中の C が Pd 副格子を維持したまま引き抜かれたことを意味しており、トポタクティックな *hcp*-Pd ナノ粒子形成を示唆している。

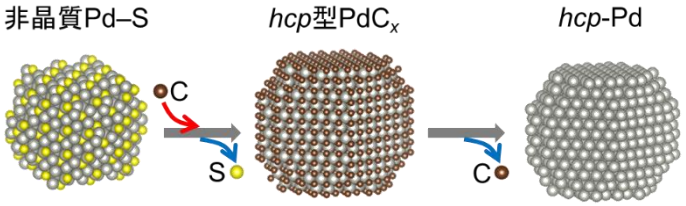

図1. *hcp*-Pd（準安定相）ナノ粒子の戦略的合成の概略図

[1] U. Mizutani *et al., Crystals* **2017**, *7*, 9. [2] S. B. Ziemecki *et al., J. Am. Chem. Soc.* **1985**, *107*, 4547.

Synthesis and localized surface plasmon resonance properties of *B*8$_1$-type anisotropic crystal structure nanoparticles

([1]*Grad. Sch. of Sci., Kyoto University*, [2]*ICR, Kyoto University,* [3]*ICAT, Hokkaido University*)
○Hyunji Lee,[1] Haruka Takekuma,[1,2] Ryota Sato,[2] Kenji Iida,[3] Toshiharu Teranishi[1,2]
Keywords: Localized surface plasmon resonance; Inorganic nanoparticles; Intermetallic compound; ordered alloy

Localized surface plasmon resonance (LSPR) of metal nanoparticles (NPs) is a unique phenomenon in which free electrons of NPs exhibit collective oscillation due to the resonance with the electric field of incident light. The spherical NPs of group 11 elements (Au, Ag, and Cu) and the alloy NPs containing group 11 elements with *fcc* (face-centered cubic)-based structure have been commonly used for LSPR in the visible region. Recently, we found that the $PtIn_2$ NPs with *C*1 (CaF_2-type) structure exhibit LSPR in the visible region[1]. Crystal structures of most plasmonic NPs are isotropic, such as *fcc* and *C*1 structures, with identical atomic arrangements along the x-, y-, and z-axes. In this study, we focused on the visible LSPR of NPs with anisotropic crystal structure, where the atomic arrangement along the z-axis differs from that of the x- and y-axes. We synthesized spherical PtSn NPs with an anisotropic *B*8$_1$ (NiAs-type) structure (inset in Fig. a), which do not contain any group 11 elements, and investigated their LSPR properties.

XRD, TEM, and HAADF-STEM measurements showed the formation of the desired spherical PtSn NPs with *B*8$_1$ structure (Fig. a,b). The obtained PtSn NPs showed two characteristic peaks in visible (ca. 380 nm) and near-infrared (ca. 850 nm) regions of the extinction spectrum (Fig. c). Both the refractive index and NPs size dependent LSPR peak shifts suggested that these peaks are derived from the LSPR. We consider that the spherical PtSn NPs exhibit two LSPRs due to their anisotropic crystal structure, especially the contribution from the two types of screening effect, i.e., the oscillation of bound *d* electrons. Calculated photoabsorption of *B*8$_1$-$Pt_{291}Sn_{306}$ NP also suggested the importance of crystal structure. Plasmonics using such anisotropic materials is expected to be a breakthrough for conventional materials.

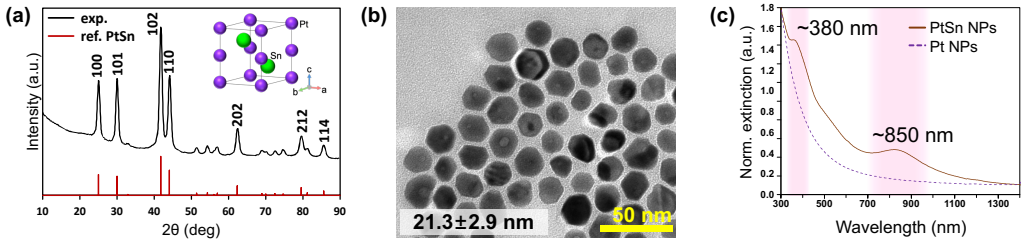

Fig. (a) XRD pattern (Inset : crystal structure) and (b) TEM image of *B*8$_1$-PtSn NPs. (c) Extinction spectra of Pt NPs and PtSn NPs.

[1] H. Takekuma, R. Sato, T. Teranishi *et al*., *Adv. Sci.*, **2024**

Centrifuge classification of citrate-stabilized silver nanoparticles and their application to SERS substrates

(*[1]Graduate School of Engineering, The University of Shiga Prefecture, [2]The University of Shiga Prefecture*) ○ Natsuki Koyama,[1] Takeo Oku,[2] Tsuyoshi Akiyama[2]

Keywords: Centrifugation·redispersion, Raman scattering, Localized surface plasmon resonance, Silver nanoparticles, Lee-Meisel method

Surface-enhanced Raman scattering (SERS) has attracted attention as a practical ultra-sensitive detection of harmful chemicals and biomarkers. SERS effect is affected by the composition and morphology of the plasmonic nanostructures. In particular, silver nanoparticles (AgNPs) are well known as an excellent SERS material[1], and are desired to improve their shape and size uniformity without ligands as SERS noise source. In this study, citrate-stabilized silver nanoparticles[2] were purified using a stepwise centrifuge classification method[3]. In addition, these purified silver nanoparticles were evaluated by their SERS performance.

The stepwise centrifuge classification method is the process repeating centrifugation and redispersion as one step (Fig.1). The centrifugation time increases by 5 minutes as the number of the step increases. The classified AgNPs obtained from the bottom of the centrifugation tube did not fuse, and their average diameter gradually decreased with increasing of the number of steps. (Fig.2). Dynamic light scattering properties and absorption spectra of the classfied AgNPs indicated that the size uniformity was improved by the classification process. The classified AgNPs were adsorbed on an amino group modified slide-glass. AgNPs on the glass substrates were evaluated by SERS spectra of rhodamine 6G. Some of the Raman scattering spectra indicated the thermal decomposition of the dye. Based on the results, the interrelationship among the SERS effect, the localized heat generated on the AgNPs, and the shape and size of the AgNPs was discussed.

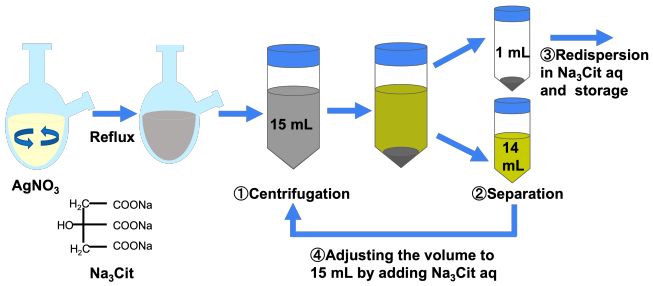

Fig. 1 The diagram of the stepwise centrifuge classification method.

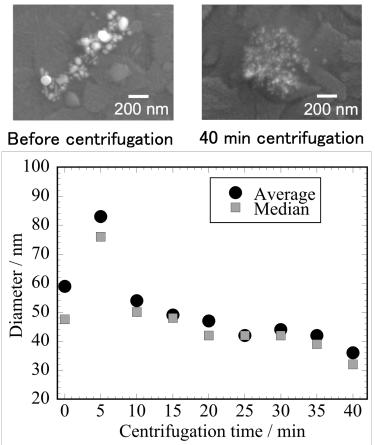

Fig. 2 SEM images and diameter of the AgNPs for centrifugation time.

1) S. Nie, S. Emory, *Science,* **1997,** 275, 1102. 2) P. C. Lee, D. Meisel, *J. Phys. Chem.,* **1982**, 86, 3391. 3) N. Koyama, T. Akiyama, T. Oku, *Jpn. J. Appl. Phys.,* **2021,** 60, 027002.

コロイドナノ粒子からの溶媒依存的な表面リガンド除去：被覆率と分散性の変化

（東京農工大）○山下 翔平、佐川 真彦、岡田 洋平
Solvent-Dependent Removal of Surface Ligands from Colloidal Nanoparticles: Changes in Coverage and Dispersibility (Tokyo University of Agriculture and Technology) ○Shohei Yamashita, Masahiko Sagawa, Yohei Okada

The synthesis and practical application of colloidal nanoparticles (NPs) require effective washing processes to remove excess surface ligands while maintaining their stability. However, current washing protocols often rely on empirical knowledge, lacking systematic understanding of how poor solvent selection affects the selective removal of different surface ligands.[1] Here, we investigate the influence of poor solvent selection on the washing process of hydrophobic colloidal NPs, focusing on the changes in the surface coverage and NPs' dispersibility. Using model systems consisting of Ag and TiO_2 NPs capped with oleic acid (OA) and/or oleylamine (OAm), we systematically evaluated various poor solvents, demonstrating that the choice of poor solvent significantly impacts the removal of OA and OAm ligands. These findings provide a rational strategy for precise control of surface ligand composition in colloidal nanoparticle systems.
Keywords: Hydrophobic nanoparticles; Ligand; Wash; Surface coverage; Dispersibility

コロイドナノ粒子の合成と実用化には、安定性を維持しながら余剰な表面リガンドを除去する効果的な洗浄プロセスが必要である。しかし、現在の洗浄プロトコルは経験的知識に依存しており、貧溶媒の選択が異なる表面リガンドの選択的除去にどのように影響するかについての系統的な理解が不足している[1]。本研究では、疎水性コロイドナノ粒子の洗浄工程における貧溶媒選択の影響について、表面被覆率および粒子分散性の変化に焦点を当てて調査した。オレイン酸（OA）またはオレイルアミン（OAm）によって被覆された銀および酸化チタンナノ粒子に対する異なる貧溶媒の効果を系統的に評価し、貧溶媒の選択が OA と OAm の選択的除去に大きく影響することを見出した。これらの知見は、コロイドナノ粒子における表面リガンド組成の精密制御に向けた合理的な戦略を提供するものである。

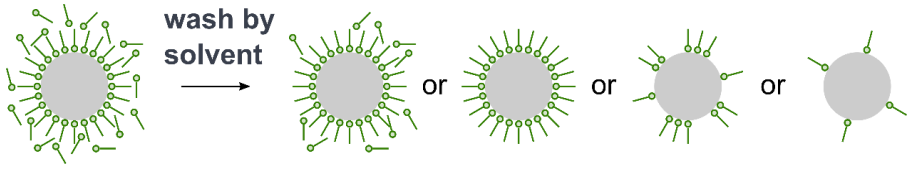

1) He, M.; Liu, X.; Liu, B.; Yang, J. *J. Colloid Interface Sci.* **2019**, *537*, 414–421.

Highly Photoluminescent $PdAu_{12}$ and $PtAu_{12}$ Clusters Protected by Bidentate N-Heterocyclic Carbenes

Dr. Dennis A. Buschmann[1,2], Dr. Shinjiro Takano[1,2], and Prof. Dr. Tatsuya Tsukuda[1,2]*

[1] Catalytic Chemistry Laboratory, Department of Chemistry, Graduate School of Science, The University of Tokyo, 7-3-1 Hongo, Bunkyo-ku, Tokyo-to, 113-0033, Japan
[2] Carbon to Metal Coating Institute, Queen's University, Kingston, Ontario, K7L 3N6, Canada
* Correspondence: tsukuda@chem.s.u-tokyo.ac.jp

The development of novel cancer therapeutics continuously drives research on nanotechnology-based immunotherapy.[1] Due to their high chemical and biostability, in combination with facile tuneable photoluminescence (PL) properties, gold nanoclusters (AuNCs) represent an ideal platform for application as bioimaging and therapy agents.[2] In recent years, N-heterocyclic carbenes (NHCs) have emerged in AuNCs as protective ligands due to their highly stabilizing properties.[3] In combination with heteroelement doping, an optimization of the PL properties is feasible,[4] which is desired in order to enhance their performance as bioimaging and therapy agents.

Here, we wish to report on the extension of the previously established synthesis of NHC-protected Au clusters toward transition-metal (M) doped NHC-AuNCs. Three different factors of PL enhancement were investigated: (1) The effect of mono- or bidentate NHCs, (2) the effects of NHC wingtip modification, and (3) the effect of heteroelement doping. The respective NHC-Au precursor complexes were co-reduced with transition metal complexes to afford cluster of the general composition $(NHC)_9MAu_{12}Cl_3$ (monodentate NHC) and $(NHC)_5MAu_{12}Cl_2$ (bidentate NHC). Depending on the type of ligand and dopant, quantum yields of >50% can be realized, which are among the highest reported for NHC-Au clusters so far.

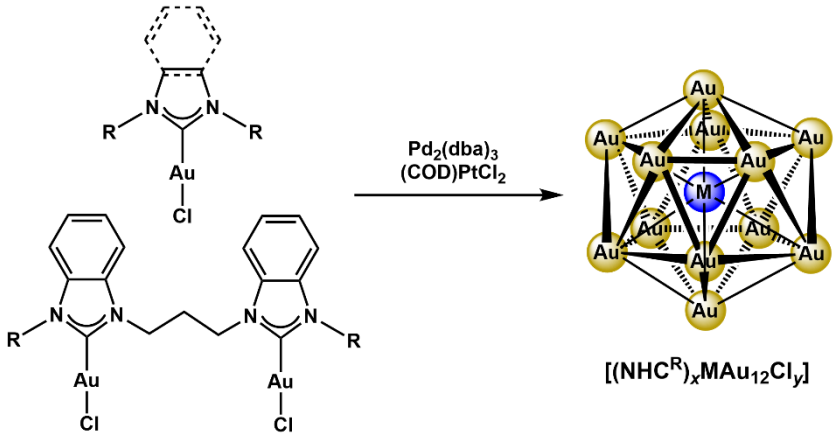

Scheme 1. Synthesis of transition-metal doped $(NHC)MAu_{12}$ clusters via co-reduction method.

References

[1] J. Lou, L. Zhang, G. Zheng, *Adv. Therap.* **2019,** *2*, 1800128. [2] C. J. Murphy *et al.*, *Acc. Chem. Res.* **2008**, *41*, 1721. [3] T. Tsukuda, C. M. Crudden *et al.*, *J. Am. Chem. Soc.* **2024**, *146*, 5759. [4] D. A. Buschmann, H. Hirai, T. Tsukuda, *Inorg. Chem. Front.* **2024**, *11*, 6694.

Phase Separation of Epsilon Iron Oxide and Barium Ferrite using a Reverse-Micelle and Sol-Gel Combined Synthesis

([1]*Graduate School of Science, The University of Tokyo*, [2] *Graduate School of Science, The University of Tsukuba*) ○Jessica Grace MacDougall,[1] Hiroko Tokoro,[2] Marie Yoshikiyo,[1] Asuka Namai,[1] Shin-ichi Ohkoshi[1]

Keywords: Barium ferrite; Epsilon iron oxide; Hard ferrite; Nanoparticles; Phase diagrams.

Hard magnetic ferrites, epsilon iron oxide (ε-Fe_2O_3) and barium ferrite ($BaFe_{12}O_{19}$) are of significant interest due to their magnetic properties and potential applications in magnetic recording media and millimetre-wave absorption. This study investigates the effect of barium ion (Ba^{2+}) to iron ion (Fe^{3+}) ratio on the synthesis of ε-Fe_2O_3 and $BaFe_{12}O_{19}$ using a combined reverse-micelle and sol-gel technique.[1,2] Reverse-micelle solutions were prepared containing $Fe(NO_3)_3$ and varying concentrations of $Ba(NO_3)_2$ (solution A), or ammonium hydroxide (solution B). Solution B was added dropwise into solution A, followed by tetraethyl orthosilicate and stirring, yielding a precipitate that was collected, annealed at 1000°C, and etched with NaOH (aq) and HCl (aq) to remove the silica matrix. By varying the Ba/Fe molar ratio, distinct phase separations and morphological changes were observed. At low Ba ion concentrations ([Ba]/[Fe] = 0.2), ε-Fe_2O_3 nanorods form predominantly, whereas higher Ba concentrations ([Ba]/[Fe] ≥ 0.4) favour the formation of $BaFe_{12}O_{19}$, shown by microscopy and powder X-ray diffraction (PXRD). At an equimolar ratio ([Ba]/[Fe] = 1), ε-Fe_2O_3 and $BaFe_{12}O_{19}$ coexist in equal proportions, with no intermediate phases. Magnetic behaviour shows reduced coercive field and increased magnetic saturation as the major phase shifts from ε-Fe_2O_3 to $BaFe_{12}O_{19}$ as the Ba ion ratio is increased.

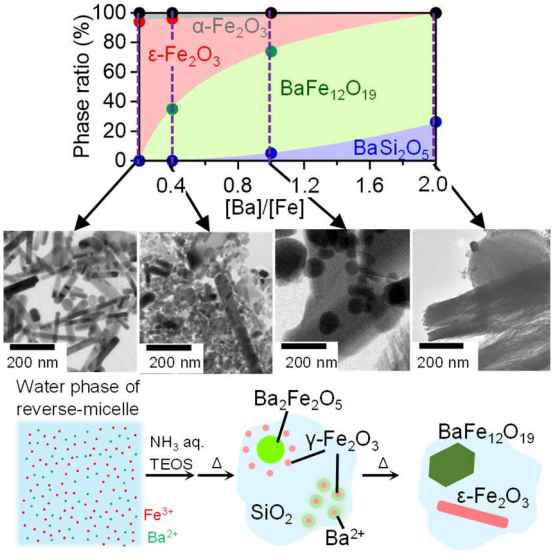

Based on the analysis conducted using scanning transmission electron microscopy coupled with energy dispersive X-ray spectroscopy and PXRD, the following mechanism is proposed for the sintering process: At 1000 °C, in areas of high barium ion concentration, γ-Fe_2O_3 nanoparticles interact with $Ba_2Fe_2O_5$ to form $BaFe_{12}O_{19}$. Conversely, in areas of low barium ion concentration, γ-Fe_2O_3 nanoparticles undergo transformation into ε-Fe_2O_3 nanorods. This study clarifies the influence of the Ba/Fe ion ratio on this synthesis, facilitating the targeted production of ferrite materials for advanced magnetic and technological applications.

1) J. MacDougall, H. Tokoro, M. Yoshikiyo, A. Namai, S. Ohkoshi, *Eur. J. Inorg. Chem.*, **2024**, *27*, e202400148. 2) J. Jin, S. Ohkoshi, K. Hashimoto, *Adv. Mater.* **2004**, *16*, 48.